

SVG360: Multi-View SVG Generation with Geometric and Color Consistency from a Single SVG

Mengnan Jiang^{1,2}, Zhaolin Sun², Christian Franke¹, Michele Franco Adesso¹, Antonio Haas^{1,3}, and Grace Li Zhang²

¹ Mercedes Benz Group

² Technische Universität Darmstadt

³ University of Stuttgart

Abstract. Scalable Vector Graphics (SVGs) are central to modern design workflows, offering scaling without distortion and precise editability. However, for single object SVGs, generating multi-view consistent SVGs from a single-view input remains underexplored. We present a three stage framework that produces multi-view SVGs with geometric and color consistency from a single SVG input. First, the rasterized input is lifted to a 3D representation and rendered under target camera poses, producing multi-view images of the object. Next, we extend the temporal memory mechanism of Segment Anything 2 (SAM2) to the spatial domain, constructing a spatial memory bank that establishes part-level correspondences across neighboring views, yielding cleaner and more consistent vector paths and color assignments without retraining. Finally, during the raster-to-vector conversion, we perform path consolidation and structural optimization to reduce redundancy while preserving boundaries and semantics. The resulting SVGs exhibit strong geometric and color consistency across views, significantly reduce redundant paths, and retain fine structural details. This work bridges generative modeling and structured vector representation, providing a scalable route to single input, object level multi-view SVG generation and supporting applications such as asset creation and semantic vector editing.

Keywords: 3D Generative Models · Novel View Synthesis · Vector Graphics Generation · Cross-view Correspondence · Spatial Representation Learning

1 Introduction

Editable vector graphics are central to modern design workflows, providing resolution independence, structural clarity, and precise editability. However, generating multi-view consistent and fully editable vector graphics for a given object remains an open challenge. When designers attempt to present an existing vector illustration from a new viewpoint, they often need to manually redraw or adjust its structure to approximate the desired perspective. This manual process is both time consuming and prone to geometric and stylistic inconsistencies.

Adobe Illustrator’s Turntable (Beta) [1] is one of the few publicly available end-to-end tools that can generate multiple views from a single 2D vector artwork. However, it offers limited control over viewing angles and discloses no technical specifications.

The task of automatically generating multi-view consistent and fully editable SVGs, however, has not been extensively explored. We define this task as synthesizing a set of path-level editable SVGs that preserve geometric and stylistic coherence across viewpoints. Solving this problem is particularly valuable for creative workflows such as turntable style visualization, multi-view logo and icon generation, and geometry consistent SVG asset editing. Bridging the gap between generative modeling and structured vector representation is therefore critical for enabling scalable and reliable design pipelines.

Recent advances in generative AI, particularly diffusion models [12, 28, 30, 32, 36, 37, 59], have enabled photorealistic and view-consistent image synthesis from a single input view, with representative approaches including a series of image-conditioned multi-view generation models [25, 26, 41, 47].

Yet, these outputs remain raster-based and lack the structured semantics and fine grained editability inherent to vector graphics. Meanwhile, existing vectorization approaches such as DiffVG [22], DeepSVG [3], and Im2Vec [34] focus on single-view reconstruction and fail to maintain geometric consistency across views. This gap motivates a core objective: enabling generative models to produce multi-view coherent and structurally editable representations in the SVG domain.

To realize this objective, we propose a unified generative to vector framework that produces multi-view, geometrically consistent, fully editable SVGs from a single input. Our method consists of three stages. It first performs 3D-aware multi-view generation to obtain geometrically plausible novel views. Then it performs cross-view refinement through spatially aligned segmentation and appearance harmonization, enhancing the consistency of object contours and colors across views in the SVG style domain. Finally, leveraging the multi-view consistent segmentation results, we perform raster-to-vector conversion followed by path consolidation and color correction, yielding compact, coherent, and easily editable multi-view SVGs.

On multi-view SVG generation, our method produces noticeably cleaner and more stable results than a strong industrial baseline. Compared with Adobe Illustrator’s Turntable, our path count deviation ($\text{RMSE}_{\text{path}}$) is about 23% lower, and the adjacent-view color count variation ($\overline{\Delta N}_{\text{color, nbr}}$) is about 86% lower. We also generate more compact SVGs, with about 7% fewer paths and about 17% fewer colors on average. In addition, our method yields smoother transitions on the yaw-pitch grid, with around 3% higher DINO feature consistency and around 2.5% higher DreamSim perceptual similarity on pitch changes [9, 31]. Finally, our vectorization module achieves high single-view fidelity measured by SSIM, LPIPS, and ΔE_{2000} [39, 50, 60]. On our single-view benchmark, it attains the lowest ΔE_{2000} among the compared raster-to-SVG baselines while maintaining a compact topology [16, 49, 51, 58].

Unified Generative to Vector Framework. We introduce an end-to-end framework to directly synthesize multi-view consistent and fully editable SVGs from a single input, bridging generative modeling with structured vector representation.

Spatially Aware Cross-View Segmentation Refinement. We design a spatially aware segmentation propagation mechanism that replaces temporal adjacency with geometry-guided neighborhood traversal, ensuring consistent part-level segmentation and enhancing SVG generation accuracy across multiple views.

Structure Preserving Vector Consolidation. We develop a vector domain consolidation strategy that merges redundant paths while maintaining semantic boundaries and structural coherence, yielding compact and semantically stable SVG assets suitable for real world design workflows.

The remainder of this paper is organized as follows: Section 2 reviews related work on multi-view SVG generation and the open gap; Section 3 presents our three stage framework; Section 4 presents experimental comparisons and ablation studies; Section 5 concludes and discusses limitations.

2 Related Work

2.1 Single-Image to 3D Vector Sketches

Such methods predict sparse 3D contour curves from single-view renders [7, 23, 48]. Lacking filled regions and explicit colors, they inevitably lose the original SVG style. Instead, we desire to generate multi-view *2D* SVGs that strictly preserve region geometry and design semantics.

2.2 Single-image to multi-view generation

Generating a turntable-like view sequence from a single reference image is a common precursor to editable multi-view SVGs. Existing approaches can be grouped into three categories.

Diffusion-based multi-view image synthesis. These methods condition 2D diffusion models on target camera poses to synthesize views in the image domain. Representative works include Zero-1-to-3 and Zero123++ [25, 41], SyncDreamer [26], and SV3D [47]. Despite strong appearance fidelity, view-wise sampling often causes geometric and color drift on thin structures and self-occlusions.

Single-image 3D reconstruction and generation. These methods infer a shared 3D asset and render novel views from the same geometry, improving multi-view consistency over 2D diffusion. Representative approaches include mesh generators (GET3D, PolyGen, MeshDiffusion) [10, 27, 29], single-image reconstruction (LRM, TripoSR, UniQue3D) [13, 44, 52], and latent 3D models (Shape-E, Trellis) [17, 53]. However, the outputs are still raster images without explicit vector paths or cross-view path correspondences.

3D Gaussian Splatting (3DGS) as a shared representation. 3DGS [18] enables efficient rendering by reprojecting a shared 3D field, often yielding stable multi-view geometry. Recent works combine diffusion priors with 3DGS for

rapid asset creation [8, 43] and extend to single-image variants [42]. Nevertheless, the results remain raster-based and require an additional vectorization stage to obtain clean, closed, and editable SVG paths.

2.3 Raster-to-Vector Generation

Converting rendered rasters into structured, editable vectors is challenging, especially when consistency must be maintained across multiple views. Classical tracing methods such as Potrace [38] and AutoTrace [51] work well for icons and low-color graphics, but often produce fragmented or redundant paths under smooth shading and complex textures.

Prior work includes optimization-based methods, e.g., DiffVG [22] which optimizes control points via differentiable rendering, and learning-based methods such as DeepSVG [3] and Im2Vec [34] built on Transformer [45] or VAE [19] designs. For raster-to-SVG conversion, LIVE [58] preserves global topology via hierarchical layers but can over-segment fine structures, while VectorFusion [16] and StarVector [49] incorporate diffusion priors or region-aware fusion for smoother paths.

Despite these advances, many pipelines still rely heavily on local pixel-level color transitions, making complex objects prone to over-fragmentation in multi-view settings. Introducing part-level segmentation before vectorization isolates coherent regions, enabling cleaner per-part conversion and more stable structure and palette behavior across views.

2.4 Segmentation and Cross-view Consistency

While semantic segmentation simplifies single-view vectorization by isolating coherent part regions, multi-view SVG generation additionally requires consistent part assignments across viewpoints. However, conventional segmentation relies on per-image pixel cues, making such consistency difficult; we therefore need a spatially stable segmentation step before vectorization to provide reliable part structures across views.

Early two-dimensional methods [5, 11, 21, 54] focus on per-image quality but do not enforce label correspondence across different views of the same object, causing boundaries to drift or merge inconsistently after projection. Foundation-scale models such as SAM, HQ-SAM, and SAM2 [4, 20, 33] provide accurate boundaries and promptable interaction, but their propagation mechanisms are primarily temporal rather than spatial, which limits consistent part correspondences across viewpoints in static 3D scenes.

Memory-based propagation in video object segmentation [6, 55] maintains features across frames to keep masks consistent over time. In multi-view settings, we can similarly view cameras as a spatial sequence on the viewing sphere, treating each view as a pseudo-temporal step and using neighboring views as spatial references.

A bridge between cross-view semantic consistency and vector-level path correspondence remains underexplored. Our approach addresses this gap by first

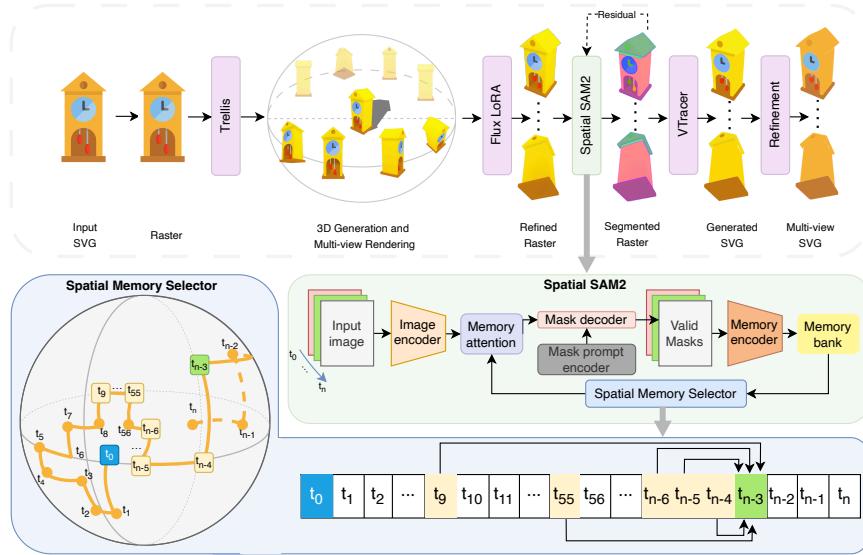


Fig. 1: Our pipeline begins by converting the input SVG into a raster image, followed by rendering 3D consistent multi-view rasters using Trellis. We then apply FLUX.1 dev [2] with a public vector-style LoRA [14] adapter (SimpleVectorFlux [35]) to harmonize their appearance. The refined rasters are processed by our **Spatial SAM2** module, which replaces temporal adjacency in SAM2 with a spatial nearest-neighbor traversal on the viewing sphere. During segmentation propagation, the **Spatial Memory Selector** retrieves the viewpoint-wise nearest memory entries. For the target view t_{n-3} , spatially adjacent views such as t_9 , t_{55} , or t_{n-6} may be closer than its temporal neighbor t_{n-4} , which helps maintain part-level consistency across viewpoints. The resulting masks are vectorized by VTracer [46] and further refined in the vector domain to produce compact, editable, and cross-view consistent multi-view SVGs.

achieving part-aware, cross-view consistent segmentation, and then leveraging these semantic units to drive compact and editable vector representations across views.

3 Method

As illustrated in Figure 1, our SVG360 framework begins with a 3D-aware rasterization stage (§3.1) that lifts a single-view SVG into geometrically plausible multi-view rasters. We then perform **spatially aligned segmentation propagation** (§3.2) to establish part-level correspondences across multi-view. Finally, the vector consolidation stage (§3.3) converts the segmented rasters into compact, fully editable multi-view SVGs with consistent geometry and color.

3.1 Multi-View Raster Generation and Harmonization

Multi-view raster generation.

Generating accurate and geometrically consistent multi-view images from a single SVG input is challenging, as purely 2D generation approaches struggle to ensure structural coherence across views. To address this, we adopt a generative 3D-based approach to synthesize multi-view images.

Although several recent single-image 3D methods (e.g., Sparc3D [24] and Hi3DGen [57]) demonstrate strong geometric fidelity, they primarily focus on precise shape reconstruction and often do not provide fully textured, render ready outputs. Such geometry-only representations are unsuitable for our color consistent raster to SVG multi-view workflow. Considering open-source availability, generation efficiency, and the level of visual fidelity required by our task, we adopt Trellis [53] as the backbone 3D generator. Trellis offers a balanced trade-off between geometric accuracy and texture consistency, and remains efficient and practical for producing coherent multi-view rasters from a single SVG input.

Trellis represents assets in a unified structured latent space and decodes them into multiple 3D formats, including meshes and 3D Gaussians [53]. Its mesh decoder builds on FlexiCubes [40], predicting per-voxel signed-distance values and extracting a watertight surface from the zero-level isosurface. While both decoders yield high-fidelity results, converting the latent to a mesh and then rasterizing from many viewpoints introduces extra discretization and baking steps, which may accumulate appearance deviations relative to the input SVG style and incur nontrivial runtime overhead. For efficiency and fidelity, we directly use the 3D Gaussian decoder and render dense multi-view rasters via Gaussian splatting, which preserves the appearance statistics needed by our downstream segmentation and vectorization stages.

Raster harmonization.

While a 3D proxy preserves global geometric consistency across viewpoints, the reconstruction can still exhibit local errors, especially along edges and curved surfaces. View-dependent illumination further introduces color variation that destabilizes raster-to-SVG conversion. We apply appearance harmonization using FLUX.1-dev [2] with a public vector-style LoRA adapter (SimpleVector-Flux [35]). The harmonized renders increase intra-region homogeneity and boundary contrast, suppress spurious shading edges, and reduce color variation across views. The resulting rasters are both view-consistent and faithful to a flat vector appearance, which improves downstream segmentation separability and stabilizes subsequent vector path consolidation.

3.2 Spatially Aligned Segmentation Propagation

After appearance harmonization, the multi-view rasters exhibit more uniform regions and sharper boundaries. To obtain cleaner and semantically stable vector paths in the subsequent vectorization stage, we need to maintain consistency of part-level identity across views. Relying on single-view segmentation alone

cannot enforce cross-view alignment of labels and boundaries, which weakens the robustness of path fitting and cross-view correspondence. Multi-view SVG generation inherently requires segmentation to be continuous in space. Accordingly, we spatialize the continuous segmentation paradigm of SAM2 by replacing temporal adjacency with spatial neighborhood on the viewing sphere and propagating masks along that sphere. Each target view is segmented under guidance from its nearest spatial neighbors, thereby maintaining part identity and boundary consistency at a global level.

Spatially Sequential Scheduling

We uniformly sample camera viewpoints on a unit sphere to obtain a globally distributed set of directions covering the entire view space. The sampling density and angular step are adjustable, allowing flexible control over the number of viewpoints and their spatial distribution according to task requirements. This configuration achieves globally balanced coverage even with a limited number of samples, forming a stable spatial adjacency structure that serves as the geometric foundation for subsequent cross-view propagation and visibility-aware reprojection.

Although the sampled views have no intrinsic temporal order, a pseudo-sequential traversal helps maintain continuity during segmentation propagation. Starting from the front view aligned with the input SVG (denoted as θ_0), each subsequent view is chosen as the unvisited one with the smallest angular distance from the current view, until all views are processed:

$$\theta_{t+1} = \arg \min_{\theta \in \text{unvisited}} d(\theta_t, \theta). \quad (1)$$

This nearest-neighbor traversal minimizes geometric discontinuities between adjacent views, producing smoother and more stable mask propagation. To measure proximity between any two viewpoints, we define their angular distance as:

$$d(\theta_i, \theta_j) = \text{atan2}(\|u_i \times u_j\|, \text{clip}(u_i \cdot u_j, -1, 1)), \quad (2)$$

where $u(\psi, \phi)$ denotes the unit viewing direction for a camera defined by horizontal rotation (yaw, ψ) and vertical rotation (pitch, ϕ):

$$u(\psi, \phi) = [\cos \phi \cos \psi, \sin \phi, \cos \phi \sin \psi]. \quad (3)$$

This atan2-based formulation is numerically more stable than arccos, particularly when two directions are nearly parallel or opposite, and directly corresponds to the great-circle distance on the unit sphere. To further enhance traversal smoothness, we apply a lightweight two-segment swap (2-opt) optimization to remove local discontinuities and maintain continuous transitions between neighboring viewpoints.

Spatial Memory Selector

After determining the traversal order, we construct a reference set for each target view to reuse information from geometrically adjacent and previously processed views. For each target view θ , we select its k nearest processed neighbors within an angular threshold τ , ensuring that the guidance originates from

Algorithm 1: Residual Discovery Loop

Input: Set of views $\{\theta_0, \dots, \theta_N\}$ with their current segmentation masks
Output: Updated mask set with newly discovered parts
 $k \leftarrow 0$; // iteration counter
 $T_{\max} \leftarrow 3$; // maximum number of passes
repeat
 for each view θ_t in spatial order **do**
 Compute uncovered foreground ratio r using the union of all masks in θ_t ;
 if $r > 5\%$ **then**
 Re-run automatic segmentation (same mode as key view),
 restricted to uncovered regions;
 Merge new masks into existing results;
 Propagate updates to neighboring views via Spatial SAM2;
 $k \leftarrow k + 1$;
until no new parts are found or $k \geq T_{\max}$;

spatially reliable local contexts. We empirically set $k = 6$ and $\tau = 75^\circ$ in all experiments. This Spatial Memory Selector mechanism, combined with the unified angular distance metric, restricts soft prompting and mask propagation to geometrically adjacent views, thereby preserving consistent part identities and boundary alignment across the entire viewing sphere.

Key Frame Initialization and Filtering. Segmentation starts from the key view θ_0 , which corresponds to the input SVG. After obtaining initial masks from the automatic segmentation model, we apply lightweight postprocessing to reduce redundancy and improve stability for subsequent propagation. We remove regions whose area is smaller than the larger of 100 pixels and 0.05% of the image area. We then apply a single morphological closing with an elliptical kernel whose size is about 0.5% of the shorter image dimension to smooth boundaries. Finally, we suppress overlapping masks using non-maximum suppression with an IoU threshold of 0.5. The cleaned masks serve as prompts for Spatial SAM2, providing stable guidance for the subsequent multi-view segmentation process.

Residual Discovery

Since the initial segmentation relies solely on the key view θ_0 , previously unseen parts that appear in other viewpoints may remain undetected. After Spatial SAM2 completes segmentation across all sampled views, we introduce a residual discovery loop to automatically detect and recover these missing regions. For each processed view θ_t , we compute the uncovered foreground ratio r based on the union of all current masks. If r exceeds 5% of the estimated foreground area, the same automatic segmentation procedure used for the key view is reactivated, but restricted to the uncovered regions. Newly discovered masks are then merged into the existing mask set and propagated to subsequent views through Spatial SAM2 to maintain cross-view consistency. The overall process is summarized in Algorithm 1.

3.3 Vector Consolidation

After segmentation, we crop each part into a transparent raster and feed it to VTracer [46], which converts pixel regions into path sets by color layering and spline fitting. Processing per part rather than per image reduces cross-part interference and yields a more compact path topology. This simplifies later consolidation and improves cross-view correspondence.

Direct vectorization often produces redundant small fills and micro strokes. We apply a light consolidation in the vector domain: sparsify colors using filled-area statistics to keep dominant colors and fold near-duplicates; clean only stroke-only micro paths to suppress artifacts from anti-aliasing; finally merge all parts within a view into a single SVG. These steps use fixed yet resolution-aware thresholds so the procedure is simple and efficient. This consolidation reduces the number of paths and colors, improves topological simplicity and editability, and yields more consistent boundaries across neighboring views.

To reduce small cross-view color drift, we extract a reference palette from the input SVG and map each source color to the nearest palette entry using the CIEDE2000 color-difference metric ΔE_{2000} [39]. We add a near-black bias to stabilize dark tones: colors in low lightness and low chroma preferentially map to black, otherwise to the closest non-black reference color. This preserves semantic colors while suppressing banding due to shadows and reflections. In practice we preserve alpha values, resolve inherited attributes into explicit colors, and remove empty attributes so that rendering is consistent across editors. Together, color alignment unifies appearance and consolidation compresses structure, improving cross-view consistency and the editability of the final SVGs.

4 Experiments

4.1 Implementation Details

For the 3D generation stage, we employ the TRELIS-image-large model to generate multi-view rasterizations from the input SVG. To harmonize the rendered appearance, we use FLUX.1-dev [2] with a public vector-style LoRA adapter (SimpleVectorFlux [14, 35]), without any additional training. We follow the adapter’s recommended trigger tokens (v3ct0r, vector) and keep a fixed prompt template across all views for consistent style. All experiments are conducted on a single NVIDIA A100-80GB PCIe GPU.

4.2 Evaluation Metrics

To comprehensively evaluate our framework, we group our metrics into three aspects. *SVG-Centric Statistics*: We evaluate the compactness of generated SVGs using the average number of paths (\bar{N}_{path}) and colors (\bar{N}_{color}). To measure structural and appearance stability relative to the input, we use $\text{RMSE}_{\text{path}}$ for path count deviation and $\Delta \bar{N}_{\text{color, nbr}}$ alongside the CIEDE2000 metric ΔE_{2000} [39]

to capture color count changes and perceptual color drift across views. *Multi-View Continuity*: For appearance continuity on the yaw-pitch viewing grid, we compute DINOv2 [31] feature consistency and DreamSim [9] perceptual similarity on adjacent view pairs. Specifically, we form yaw-adjacent pairs by grouping views with the same pitch and consecutive yaw steps, and pitch-adjacent pairs by grouping views with the same yaw and consecutive pitch levels. We report Yaw and Pitch by averaging scores over the corresponding adjacent pairs, and Overall by averaging over all adjacent pairs on the grid. *Single-View Fidelity*: We use standard image quality metrics, SSIM [50] and LPIPS [60], to evaluate the fundamental raster-to-SVG reconstruction quality. Detailed mathematical formulations and computation specifics for all aforementioned metrics are provided in the supplementary material.

4.3 Comparison

Baselines.

For multi-view generation, Adobe Illustrator’s Turntable (Beta) [1] serves as our primary industrial baseline. It is a commercial, publicly available end-to-end feature that generates multi-view SVGs from a single 2D vector artwork. Its internal implementation, view grid, and technical specifications are not disclosed, and no programmatic interface is provided. According to the official documentation, Turntable supports approximately $\pm 120^\circ$ horizontal rotation in yaw (sampled every 15°) and three pitch levels at $\{-45^\circ, 0^\circ, +45^\circ\}$. For a fair comparison, we adopt the exact same camera poses defined by the Turntable configuration in our experiments. Since Adobe Turntable lacks an API and necessitates manual per-view export, large-scale evaluation is not practical to scale. To ensure rigorous comparison, we curated a representative benchmark of 30 SVGs across categories like vehicles, buildings, and animals. By fully exporting the 51-view yaw-pitch grid for each, we obtained a dense set of 1530 multi-view SVG outputs for strict quantitative and qualitative evaluation. For single view vectorization, we additionally benchmark our vectorization module on a small set of 200 simple single object SVGs and compare against LIVE [58], StarVector [49], and AutoTrace [51].

Quantitative Comparison.

Multi-View SVG Statistics. Table 1 compares the intrinsic properties of generated SVGs. Our approach produces highly compact vectors (avg. 20.77 paths, 3.65 colors) while demonstrating exceptional stability across viewpoints. Compared to Adobe Turntable, we reduce path count deviation ($\text{RMSE}_{\text{path}}$) from 14.22 to 10.95. Color stability improvements are particularly striking: we reduce adjacent-view color count variation ($\Delta \bar{N}_{\text{color, nbr}}$) from 2.01 to 0.29, and perceptual color drift (ΔE_{2000}) from 3.22 to 1.19, substantially reducing the structural flickering and color inconsistencies common in the baseline.

Multi-View Continuity. Table 2 evaluates spatial continuity across the yaw-pitch viewing grid. Overall, our approach yields more coherent view-to-view transitions than Adobe Turntable. While Turntable attains competitive perceptual

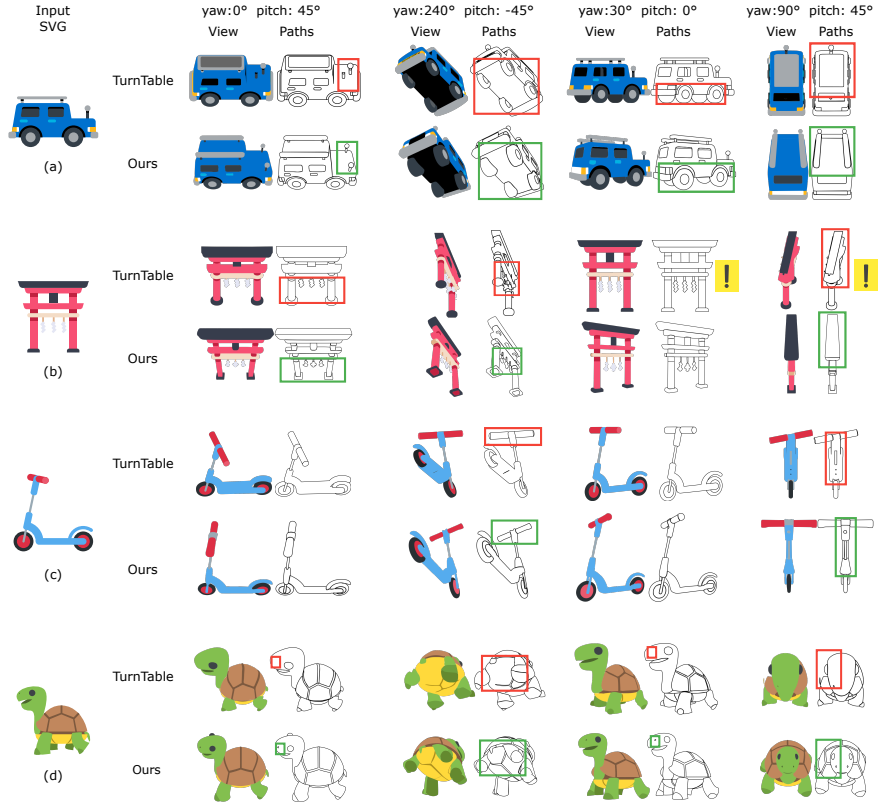


Fig. 2: Qualitative comparison with Adobe Turntable. Target camera poses (yaw and pitch) are annotated at the top; ! marks views that deviate from the target pose. **(a)** Car: unrealistic structural changes (e.g., incomplete or misplaced headlights) and inconsistent foreshortening/scale (e.g., wheels vs. chassis). **(b)** Torii gate: slender hanging components suffer from path crowding and tangling in certain views. **(c)** Scooter: distorted handlebar proportions in oblique views and structural inconsistency around the steering tube (head-tube region). **(d)** Turtle: missing small parts (e.g., nose) and locally incomplete shell regions in challenging views.

scores on simple yaw rotations, our method is more robust on the full grid, achieving higher overall DINO consistency (0.8864 vs. 0.8611). Overall DreamSim is comparable (0.8392 vs. 0.8388), but the advantage becomes clear under challenging pitch changes, where our method achieves higher Pitch DreamSim (0.7748 vs. 0.7563), indicating smoother appearance transitions across viewpoints.

Single-View Raster-to-SVG Fidelity. Table 3 validates our vectorization module against state-of-the-art models. Our method yields the highest visual fidelity (SSIM: 0.926, LPIPS: 0.020, ΔE_{2000} : 0.408) while striking an optimal balance in structural compactness. Specifically, while StarVector produces slightly

Table 1: SVG-centric multi-view comparison against Adobe Turntable. We report statistics of the generated multi-view SVGs, including compactness (fewer paths/colors indicate a more compact and editable SVG) and cross-view stability derived from SVG structure and palette behavior. Lower $\text{RMSE}_{\text{path}}$, $\overline{\Delta N}_{\text{color, nbr}}$, and ΔE_{2000} indicate more stable structure and color across views.

Method	Compactness		SVG structure	Color consistency	
	$\overline{N}_{\text{path}}$	$\overline{N}_{\text{color}}$	$\text{RMSE}_{\text{path}} \downarrow$	$\overline{\Delta N}_{\text{color, nbr}} \downarrow$	$\Delta E_{2000} \downarrow$
Adobe Turntable	22.34	4.41	14.22	2.01	3.22
Ours	20.77	3.65	10.95	0.29	1.19

Table 2: Multi view continuity comparison against Adobe Turntable on a yaw and pitch camera grid. We measure local transition smoothness between adjacent views using DINOv2 feature consistency and DreamSim perceptual similarity, reporting yaw, pitch, and overall scores.

Method	DINO Consistency			DreamSim Similarity		
	Yaw \uparrow	Pitch \uparrow	Overall \uparrow	Yaw \uparrow	Pitch \uparrow	Overall \uparrow
Adobe Turntable	0.9005	0.8053	0.8611	0.8973	0.7563	0.8388
Ours	0.9074	0.8567	0.8864	0.8848	0.7748	0.8392

Table 3: Single-view (initial input view) raster-to-SVG comparison. We render predicted SVGs back to rasters and evaluate against the input raster.

Method	SSIM \uparrow	LPIPS \downarrow	$\Delta E_{2000} \downarrow$	Paths
LIVE [58]	0.803	0.065	7.364	18.2
StarVector [49]	0.697	0.153	17.706	15.2
AutoTrace [51]	0.812	0.063	2.792	448.2
Ours	0.926	0.020	0.408	19.75

fewer paths (15.2) at the cost of poor fidelity (ΔE_{2000} : 17.706), and AutoTrace yields reasonable similarity (SSIM: 0.812) but heavily fragmented topology (448.2 paths), our method avoids these trade-offs, delivering near-perfect reconstruction with only 19.75 paths.

Qualitative Comparison.

Figure 2 provides a visual comparison with Adobe Turntable. Overall, the baseline often struggles to maintain cross-view 3D consistency for single-SVG multi-view generation. It is prone to geometric/foreshortening distortions, cluttered paths on thin or overlapping structures, and occasional pose drift. Under challenging viewpoints, it may also miss small semantic parts. In contrast, by leveraging an explicit 3D representation with strict pose control, our approach maintains more stable geometry, cleaner part separation, and coherent multi-view appearances.

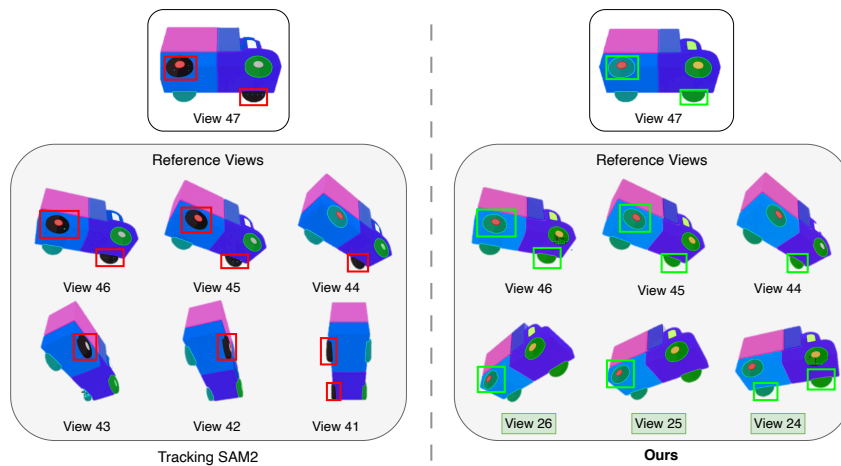


Fig. 3: Segmentation comparison between the original SAM2 tracking mode (left) and Spatial SAM2 (ours, right) at view 47. For each method, we show the six reference views used for memory support. Tracking SAM2 uses views 41-46, while Spatial SAM2 uses views 24-26, and 44-46. Results correspond to the first iteration before any subsequent refinement.

4.4 Ablation Study

Figure 3 illustrates the difference between the original Tracking SAM2 (Video Segmentation) and our Spatial SAM2 when propagating masks across multi-view settings. The propagation mechanism of Tracking Mode SAM2 is fundamentally linear and one-directional: it progresses strictly along the view sequence and therefore relies on the temporally adjacent set of reference views (views 41–46). While such linear propagation is appropriate in video scenarios, it introduces a notable limitation in static multi-view renderings. If certain structures are not robustly tracked over several consecutive views, the resulting errors accumulate and become amplified along the propagation chain. Consequently, at views with large spatial offsets, the tracking mode frequently fails to recover local structures such as wheels, leading to partial or complete omission.

Our Spatial SAM2, in contrast, does not depend on single-direction propagation. Instead, it selects reference views based on true geometric proximity on the viewing sphere. Besides leveraging temporally adjacent views such as 44–46, it also incorporates views like 24–26, which may be far apart in the temporal order but remain spatially close to the target view. Since reference information is validated jointly across multiple spatial neighbors rather than flowing along a single temporal chain, Spatial SAM2 effectively suppresses error accumulation and enhances segmentation robustness. As a result, even at spatially distant viewpoints, structures such as wheels remain stable and consistently segmented across views.

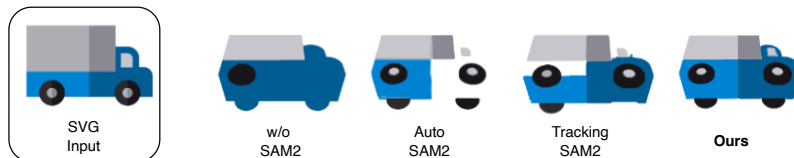


Fig. 4: Ablation study of four segmentation strategies: Spatial SAM2 (ours), SAM2 Tracking Mode, SAM2 Auto Mode, and a segmentation-free VTracer baseline.

As shown in Figure 4, we further compare the impact of four segmentation strategies on the final SVG outputs. Spatial SAM2 produces the most stable and coherent results. The tracking mode of SAM2 still exhibits occasional misses in certain viewpoints. The Auto mode (i.e., SAM2’s Segment Everything) tends to over-fragment continuous structures due to the lack of cross-view constraints, resulting in inconsistent topology across views. When segmentation is entirely omitted, many parts fail to survive the vectorization stage and cannot be reliably reconstructed, leaving only a few coarse contours. These findings confirm that enforcing spatially consistent segmentation is critical for producing high-quality multi-view SVGs.

5 Conclusion

We presented a unified generative-to-vector framework that produces geometrically consistent and fully editable multi-view SVGs from a single input illustration. By integrating 3D-aware multi-view generation, spatially aligned cross-view refinement, and vector-domain consolidation, our approach bridges raster-based synthesis with structured vector representations and enables practical multi-view SVG editing workflows.

Despite these improvements, several challenges remain. Part-level consistency is still constrained by the limitations of current segmentation models, particularly on objects with intricate topology or numerous fine-grained components. Our framework currently focuses on single-object inputs and does not yet extend to scene-level vector graphics requiring instance reasoning or world-coordinate camera transformations. Furthermore, vectorization remains most reliable for closed, well-formed paths, while open or stroke-only structures provide weaker cues for stable multi-view reconstruction.

These limitations suggest promising directions for future work, including stronger segmentation priors, more robust cross-view correspondence strategies, scene-level vector generation, and topology-aware handling of open-path SVGs. Beyond these extensions, we also see opportunities to better exploit vector-specific structure, e.g., enforcing cross-view consistency of palettes and layer hierarchies.

References

1. Adobe Research: View 2d objects from new angles — illustrator (2025), <https://helpx.adobe.com/illustrator/desktop/use-generative-ai/view-artwork-from-any-angle.html>, official HelpX page for Illustrator Turntable (Beta). Last updated: Oct. 27, 2025
2. Black Forest Labs: Flux: Foundation models for universal image generation. <https://blackforestlabs.ai> (2024), accessed: 2025-01-10
3. Carlier, A., Couprie, C., Verbeek, J.: Deepsvg: A hierarchical generative network for vector graphics animation. In: *NeurIPS* (2020)
4. Cheng, B., Girdhar, R., Misra, I.: Hq-sam: Improving the segmentation anything model with high-quality data. *arXiv preprint arXiv:2306.01567* (2023)
5. Cheng, B., Misra, I., Schwing, A., Kirillov, A., Girdhar, R.: Mask2former: Masked-attention transformer for universal image segmentation. In: *CVPR*. pp. 12829–12839 (2022)
6. Cheng, H.K., Tai, Y.W., Tang, C.K.: Stcn: Spatio-temporal contrastive learning for video object segmentation. In: *NeurIPS* (2021)
7. Choi, C., Lee, J., Park, J., Kim, Y.M.: 3doodle: Compact abstraction of objects with 3d strokes. *ACM Transactions on Graphics* **43**(4) (jul 2024). <https://doi.org/10.1145/3658156>
8. Chu, F., et al.: Gaussiandreamer: Fast generation from text to 3d gaussians. *arXiv preprint arXiv:2311.11284* (2023)
9. Fu, S., Tamir, N., Sundaram, S., Chai, L., Zhang, R., Dekel, T., Isola, P.: DreamSim: Learning new dimensions of human visual similarity using synthetic data. In: *NeurIPS* (2023)
10. Gao, J., et al.: Get3d: A generative model of high quality 3d textured shapes learned from images. In: *NeurIPS* (2022)
11. He, K., Gkioxari, G., Dollár, P., Girshick, R.: Mask r-cnn. In: *ICCV*. pp. 2961–2969 (2017)
12. Ho, J., Jain, A., Abbeel, P.: Denoising diffusion probabilistic models. In: *NeurIPS* (2020)
13. Hong, Y., Zhang, K., Gu, J., Bi, S., Zhou, Y., Liu, D., Liu, F., Sunkavalli, K., Bui, T., Tan, H.: LRM: Large reconstruction model for single image to 3D. *arXiv preprint arXiv:2311.04400* (2023)
14. Hu, E.J., Shen, Y., Wallis, P., Allen-Zhu, Z., Li, Y., Wang, S., Wang, L., Chen, W.: Lora: Low-rank adaptation of large language models. In: *ICLR* (2022)
15. Huang, Z., Guo, Y.C., Wang, H., Yi, R., Ma, L., Cao, Y.P., Sheng, L.: Mv-adapter: Multi-view consistent image generation made easy. *arXiv preprint arXiv:2412.03632* (2024)
16. Jain, A., Xie, A., Abbeel, P.: Vectorfusion: Text-to-svg by abstracting pixel-based diffusion models. In: *CVPR*. pp. 1911–1920 (2022)
17. Jun, H., Nichol, A., et al.: Shap-e: Generating conditional 3d implicit functions. *arXiv preprint arXiv:2305.02463* (2023)
18. Kerbl, B., Kopanas, G., Leimkühler, T., Drettakis, G.: 3d gaussian splatting for real-time radiance field rendering. In: *ACM SIGGRAPH* (2023)
19. Kingma, D.P., Welling, M.: Auto-encoding variational bayes. In: *International Conference on Learning Representations* (2014)
20. Kirillov, A., Mintun, E., Ravi, N., Mao, H., Rolland, C., Gustafson, L., Whitehead, S., Berg, A.C., Lo, W.Y., Dollár, P., Girshick, R.: Segment anything. In: *ICCV* (2023)

21. Li, F., Zhang, H., Sun, P., Lin, E., Zou, X., Yang, J., Zhang, L., Gao, J.: Maskdino: Towards a unified transformer-based framework for object detection and segmentation. In: CVPR (2023)
22. Li, T.M., Lukáč, M., Gharbi, M., Ragan-Kelley, J.: Diffvg: Differentiable vector graphics rasterization for editing and learning. ACM TOG **39**(6), 193:1–193:15 (2020)
23. Li, Y., Xiao, J., Lu, Z., Wang, Y., Jiang, H.: Empowering vector graphics with consistently arbitrary viewing and view-dependent visibility. In: Proceedings of the IEEE/CVF Conference on Computer Vision and Pattern Recognition (CVPR). pp. 18531–18540 (jun 2025)
24. Li, Z., Wang, Y., Zheng, H., Luo, Y., Wen, B.: Sparc: Sparse representation and construction for high-resolution 3d shapes modeling. arXiv preprint arXiv:2505.14521 (2025), <https://arxiv.org/abs/2505.14521>
25. Liu, R., et al.: Zero-1-to-3: Zero-shot one image to 3d object. In: ICCV (2023)
26. Liu, Y., et al.: Syncdreamer: Generating multiview consistent images from a single view. In: ICLR (2024)
27. Liu, Z., Feng, Y., Black, M.J., Nowrouzezahrai, D., Paull, L., Liu, W.: Meshdiffusion: Score-based generative 3d mesh modeling. In: ICLR (2023), <https://openreview.net/forum?id=OcpM2ApF9p6>
28. Mou, C., Wang, X., Xie, L., Wu, Y., Zhang, J., Qi, Z., Shan, Y., Qie, X.: T2i-adapter: Learning adapters to dig out more controllable ability for text-to-image diffusion models. arXiv preprint arXiv:2302.08453 (2023), <https://arxiv.org/abs/2302.08453>
29. Nash, C., et al.: Polygen: An autoregressive generative model of 3d meshes. In: ICML (2020)
30. Nichol, A., Dhariwal, P., Ramesh, A., Shyam, P., Mishkin, P., McGrew, B., Sutskever, I., Chen, M.: Glide: Towards photorealistic image generation and editing with text-guided diffusion models. arXiv preprint arXiv:2112.10741 (2021), <https://arxiv.org/abs/2112.10741>
31. Oquab, M., Darcet, T., Moutakanni, T., Voita, H., Sors, M., et al.: DINOv2: Learning robust visual features without supervision. arXiv preprint arXiv:2304.07193 (2023)
32. Ramesh, A., Dhariwal, P., Nichol, A., Chu, C., Chen, M.: Hierarchical text-conditional image generation with clip latents. arXiv preprint arXiv:2204.06125 (2022), <https://arxiv.org/abs/2204.06125>
33. Ravi, N., Kirillov, A., Dollár, P., Girshick, R.: Sam 2: Segment anything in images and videos. arXiv preprint arXiv:2408.00714 (2024)
34. Reddy, P., Liu, J., Cole, F., Pfister, H., Zitnick, C.L., Freeman, W.T., Freeman, D.M.: Im2vec: Synthesizing vector graphics without vector supervision. In: CVPR. pp. 7342–7351 (2021)
35. renderartist: Simplevectorflux: Simple vector flux lora. <https://huggingface.co/renderartist/simplevectorflux> (2024), loRA adapter for FLUX.1 dev. Trigger words: v3ct0r, vector. License: CreativeML OpenRAIL M. Accessed: 2026-03-04
36. Rombach, R., Blattmann, A., Lorenz, D., Esser, P., Ommer, B.: High-resolution image synthesis with latent diffusion models. In: CVPR. pp. 10674–10685 (2022). <https://doi.org/10.1109/CVPR52688.2022.01042>, https://openaccess.thecvf.com/content/CVPR2022/html/Rombach_High-Resolution_Image_Synthesis_With_Latent_Diffusion_Models_CVPR_2022_paper.html
37. Saharia, C., Chan, W., Saxena, S., Li, L., Whang, J., Denton, E., Ghasemipour, S.K.S., Ayan, B.K., Mahdavi, S.S., Lopes, R.G., Salimans, T., Ho, J., Fleet, D.J.,

- Norouzi, M.: Photorealistic text-to-image diffusion models with deep language understanding. arXiv preprint arXiv:2205.11487 (2022), <https://arxiv.org/abs/2205.11487>
38. Selinger, P.: Potrace: a polygon-based tracing algorithm. <https://potrace.sourceforge.net/potrace.pdf> (2003)
 39. Sharma, G., Wu, W., Dalal, E.N.: The ciede2000 color-difference formula: Implementation notes, supplementary test data, and geometric byproducts. *Color Research & Application* **30**(1), 21–30 (2005)
 40. Shen, T., Munkberg, J., Hasselgren, J., Yin, K., Wang, Z., Chen, W., Gojcic, Z., Fidler, S., Sharp, N., Gao, J.: Flexible isosurface extraction for gradient-based mesh optimization. *ACM TOG* **42**(4) (2023). <https://doi.org/10.1145/3592430>, <https://arxiv.org/abs/2308.05371>
 41. Shi, R., et al.: Zero123++: a single image to consistent multi-view diffusion base model. arXiv:2310.15110 (2023)
 42. Szymanowicz, S., et al.: Splatter image: Ultra-fast single-image to 3d with gaussian splatting. In: CVPR (2024)
 43. Tang, J., et al.: Dreamgaussian: Generative gaussian splatting for efficient 3d content creation. arXiv preprint arXiv:2309.16653 (2023)
 44. Tochilkin, D., Pankratz, D., Liu, Z., Huang, Z., , Letts, A., Li, Y., Liang, D., Laforte, C., Jampani, V., Cao, Y.P.: Triposr: Fast 3d object reconstruction from a single image. arXiv preprint arXiv:2403.02151 (2024)
 45. Vaswani, A., Shazeer, N., Parmar, N., Uszkoreit, J., Jones, L., Gomez, A.N., Kaiser, Ł., Polosukhin, I.: Attention is all you need. In: *Advances in Neural Information Processing Systems* (2017)
 46. VisionCortex Project: Vtracer: A fast, vector-based image tracing engine. <https://www.visioncortex.org/vtracer/> (2023), accessed: 2025-10-30
 47. Voleti, V., et al.: Sv3d: Stable video 3d for novel multi-view synthesis and 3d generation. arXiv:2403.12008 (2024)
 48. Wang, C., Zhou, H., Luo, L., Yu, Q.: Viewcraft3d: High-fidelity and view-consistent 3d vector graphics synthesis. In: *Advances in Neural Information Processing Systems (NeurIPS)* (2025), <https://openreview.net/forum?id=5fAtzK3hBd>, neurIPS 2025 Poster
 49. Wang, T., Liu, Z., Zhang, H., Yu, D., Liao, J.: Starvector: Structure-aware vectorization via region fusion and diffusion priors. In: CVPR (2024)
 50. Wang, Z., Bovik, A.C., Sheikh, H.R., Simoncelli, E.P.: Image quality assessment: from error visibility to structural similarity. *IEEE TIP* **13**(4), 600–612 (2004)
 51. Weber, M., et al.: AutoTrace: A program for converting bitmap to vector graphics. <http://autotrace.sourceforge.net/> (2001)
 52. Wu, K., Liu, F., Cai, Z., Yan, R., Wang, H., Hu, Y., Duan, Y., Ma, K.: Unique3d: High-quality and efficient 3d mesh generation from a single image. In: *NeurIPS* (2024)
 53. Xiang, J., Lv, Z., Xu, S., Deng, Y., Wang, R., Zhang, B., Chen, D., Tong, X., Yang, J.: Structured 3d latents for scalable and versatile 3d generation. arXiv preprint arXiv:2412.01506 (2024)
 54. Xie, E., Wang, W., Yu, Z., Anandkumar, A., Alvarez, J.M., Luo, P.: Segformer: Simple and efficient design for semantic segmentation with transformers. In: *NeurIPS* (2021)
 55. Yang, J., Wu, W., Chen, S., Xie, L., Tian, Q.: Deaot: Memory-efficient decoupled attention for online video object segmentation. In: CVPR (2023)

56. Yang, X., Shi, H., Zhang, B., Yang, F., Wang, J., Zhao, H., Liu, X., Wang, X., Lin, Q., Yu, J., et al.: Hunyuan3d 1.0: A unified framework for text-to-3d and image-to-3d generation. arXiv preprint arXiv:2411.02293 (2024)
57. Ye, C., Wu, Y., Lu, Z., Chang, J., Guo, X., Zhou, J., Zhao, H., Han, X.: Hi3dgen: High-fidelity 3d geometry generation from images via normal bridging. In: ICCV (2025), https://openaccess.thecvf.com/content/ICCV2025/papers/Ye_Hi3DGen_High-fidelity_3D_Geometry_Generation_from_Images_via_Normal_Bridging_ICCV_2025_paper.pdf
58. Yue, J., Chen, K., Xu, Y., Yu, Q.: Live: Layer-wise image vectorization for structure-preserving vector graphics. ACM TOG (2024)
59. Zhang, L., Rao, A., Agrawala, M.: Adding conditional control to text-to-image diffusion models. In: ICCV. pp. 3813–3824 (2023), https://openaccess.thecvf.com/content/ICCV2023/papers/Zhang_Adding_Conditional_Control_to_Text-to-Image_Diffusion_Models_ICCV_2023_paper.pdf
60. Zhang, R., Isola, P., Efros, A.A., Shechtman, E., Wang, O.: The unreasonable effectiveness of deep features as a perceptual metric. In: CVPR. pp. 586–595 (2018)

Supplementary Material

A Implementation Details

Our full system consists of three main stages: (1) single-SVG-conditioned multi-view image generation, (2) cross-view part-aware segmentation and propagation, and (3) single-view raster-to-SVG vectorization for each generated view.

3D Generation and Harmonization. For the multi-view raster generation, we employ the TRELLIS-image-large model [53] as our 3D prior. To harmonize the rendered appearance and reduce view-dependent shading artifacts, we use FLUX.1-dev [2] combined with the SimpleVector Flux [35] LoRA [14] adapter. We set the inference steps for FLUX to 20 with a guidance scale (CFG) of 3.5. To maintain a consistent SVG style across all viewpoints, we use a fixed prompt template: “A clean vector illustration of a [object class], flat colors, v3ct0r, vector style, white background”.

Spatial SAM2 and Vector Consolidation. In the Spatial SAM2 module [33], we set the neighborhood size for the Spatial Memory Selector to $k = 6$ and the angular threshold to $\tau = 75^\circ$. During the vector consolidation stage, regions with an area smaller than 100 pixels (or 0.05% of the image area, whichever is larger) are treated as noise and filtered out. To resolve stroke artifacts from anti-aliasing, we explicitly correct hue and brightness deviations by mapping source colors to the nearest reference palette entry using the CIEDE2000 metric (ΔE_{2000}) [39].

B Additional Experiments and Comparisons

B.1 Comparison with Multi-View Image Generators

While our primary goal is multi-view SVG generation, the geometric stability of the intermediate multi-view rasters is crucial. In Figure S1, we qualitatively compare our 3D-guided rendering approach, which utilizes the TRELLIS-image-large [53] model as a 3D prior, against state-of-the-art multi-view image generators: Hunyuan3D [56], MV-Adapter [15], and Zero123++ [41].

B.2 Qualitative Vectorization Comparison

We provide qualitative comparisons corresponding to the single-view raster-to-SVG fidelity evaluation (Table 3 in the main text). Figure S2 presents the vectorization results of identical input raster images. Recent learning-based baselines

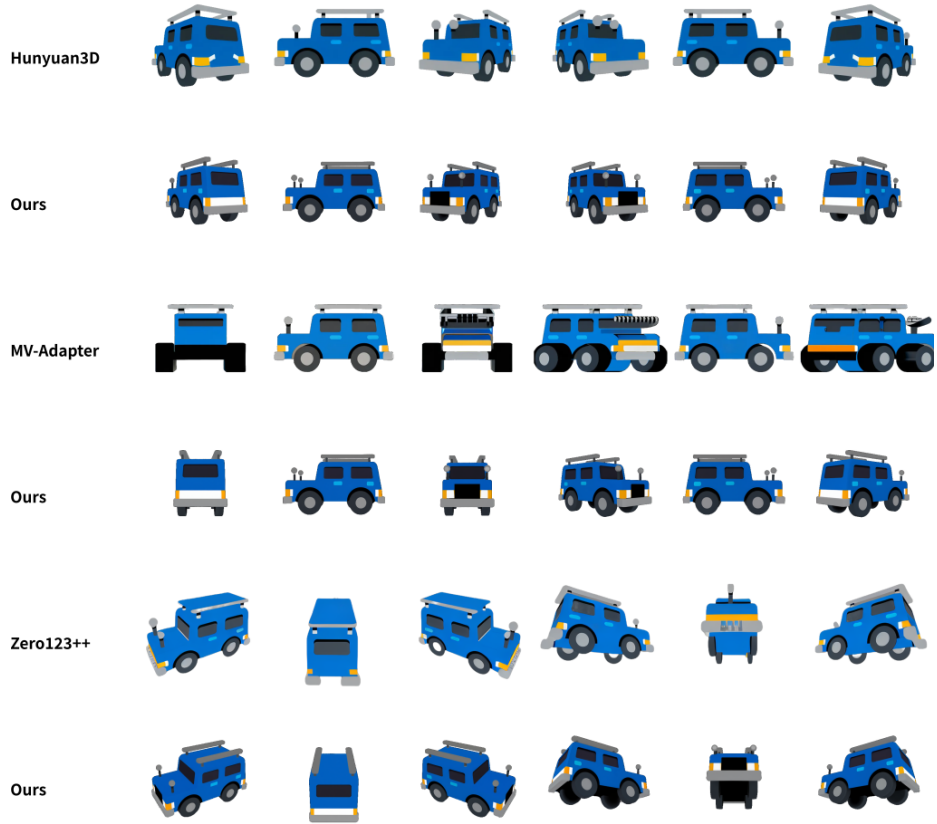


Fig. S1: Qualitative comparison of multi-view image generation. Baselines exhibit strong view-dependent distortions and shading drift, whereas our method (based on TRELIS [53]) maintains coherent structure and stable appearance.

exhibit distinct artifacts: LIVE [58] produces blurry edges and color bleeding, while StarVector [49] merges neighboring regions excessively, losing local contrast. Classical methods like AutoTrace [51] fragment smooth color fields into thousands of polygons, resulting in noisy outlines. In comparison, our vectorization module, which leverages part-aware segmentation and topological consolidation, delivers clean, visually consistent SVGs with accurate color boundaries and minimal redundancy.

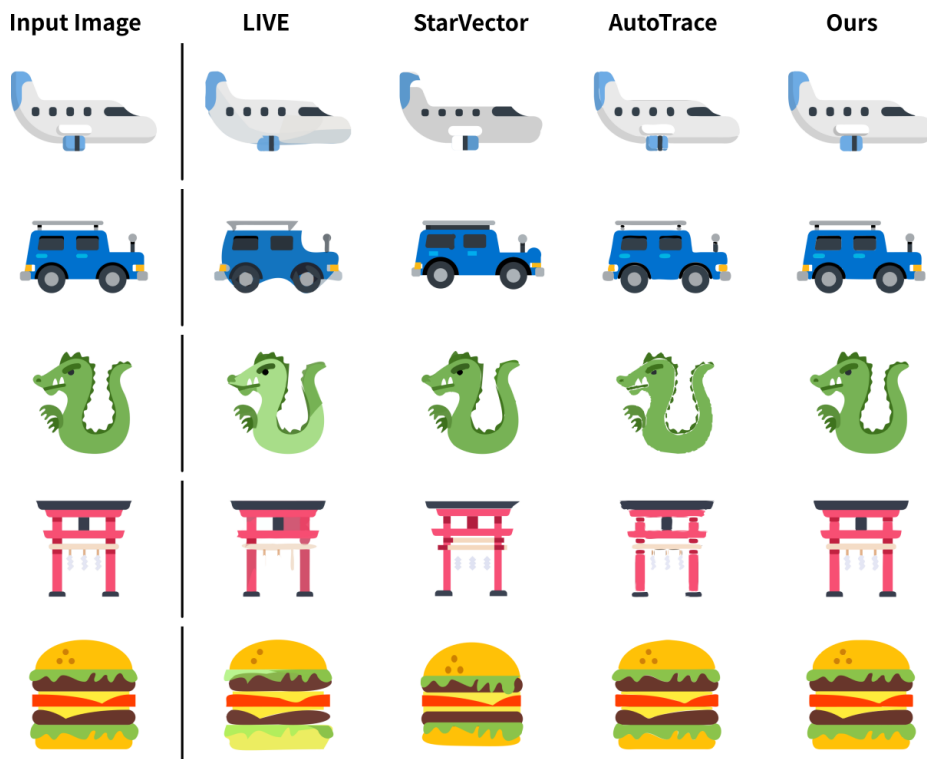


Fig. S2: Qualitative vectorization results under identical viewpoints. Our method delivers clean SVGs with accurate color boundaries, whereas baselines suffer from blurry edges, color bleeding, or severe polygon fragmentation.

C Analysis of Key Modules

C.1 Visual Analysis of Appearance Harmonization

We first examine the role of appearance harmonization in our pipeline. As shown in Figure S3, raw 3D renderings often exhibit view-dependent shading variations,

local intensity gradients, and mild chromatic inconsistencies. Although these artifacts do not alter the underlying geometry, they introduce appearance noise that can interfere with downstream segmentation and raster-to-SVG conversion.

After refinement with FLUX.1-dev [2] and the public vector-style LoRA adapter (SimpleVectorFlux [14, 35]), the rendered views become closer to a flat vector-style appearance while preserving the original object structure. The difference maps are concentrated primarily around shading regions, and the consistently high SSIM scores indicate that the refinement mainly affects appearance rather than geometry. In practice, this harmonization improves intra-region uniformity, sharpens region boundaries, and suppresses spurious shading edges, thereby making subsequent segmentation more reliable and the following vector consolidation more stable across viewpoints.

C.2 Single-View Evidence for Segmentation-Guided Vector Consolidation

We next examine the effect of our vectorization stage in the single-view setting. This analysis complements the multi-view results by showing that the same design also improves SVG reconstruction quality for individual views. To make this effect explicit, we compare our full pipeline with a direct raster-to-vector baseline.

Specifically, we use direct VTracer as the baseline, where the entire image is vectorized globally without part-aware masks or explicit palette alignment. This provides a meaningful reference because VTracer is also the tracing backend used in our method. The comparison therefore highlights the benefit of the additional design choices introduced by our pipeline, rather than differences in the underlying tracer itself.

As shown in the path-line visualizations in Figure S4, direct raster-to-vector conversion remains sensitive to anti-aliasing artifacts and sub-pixel color variation, often producing fragmented micro-paths, overlapping boundaries, and locally unstable topology. In contrast, our full pipeline yields cleaner path layouts and sharper region boundaries.

These improvements arise from the combined effect of three design choices. First, part-aware segmentation decomposes the raster input into structurally meaningful regions before tracing. Second, region-wise vectorization reduces cross-part interference and prevents paths from crossing semantic boundaries. Third, palette alignment maps traced colors back to the reference SVG palette, suppressing residual chromatic noise and improving color faithfulness.

Table S1 summarizes the quantitative comparison. Relative to direct VTracer, our full pipeline improves SSIM from 0.833 to 0.926, reduces LPIPS from 0.0206 to 0.0200, and substantially lowers perceptual color drift (ΔE_{2000}) from 1.340 to 0.408, while also slightly reducing the average number of paths from 20.4 to 19.75. These results indicate that the proposed vector consolidation strategy contributes not only to multi-view consistency, but also to high-fidelity single-view SVG reconstruction.

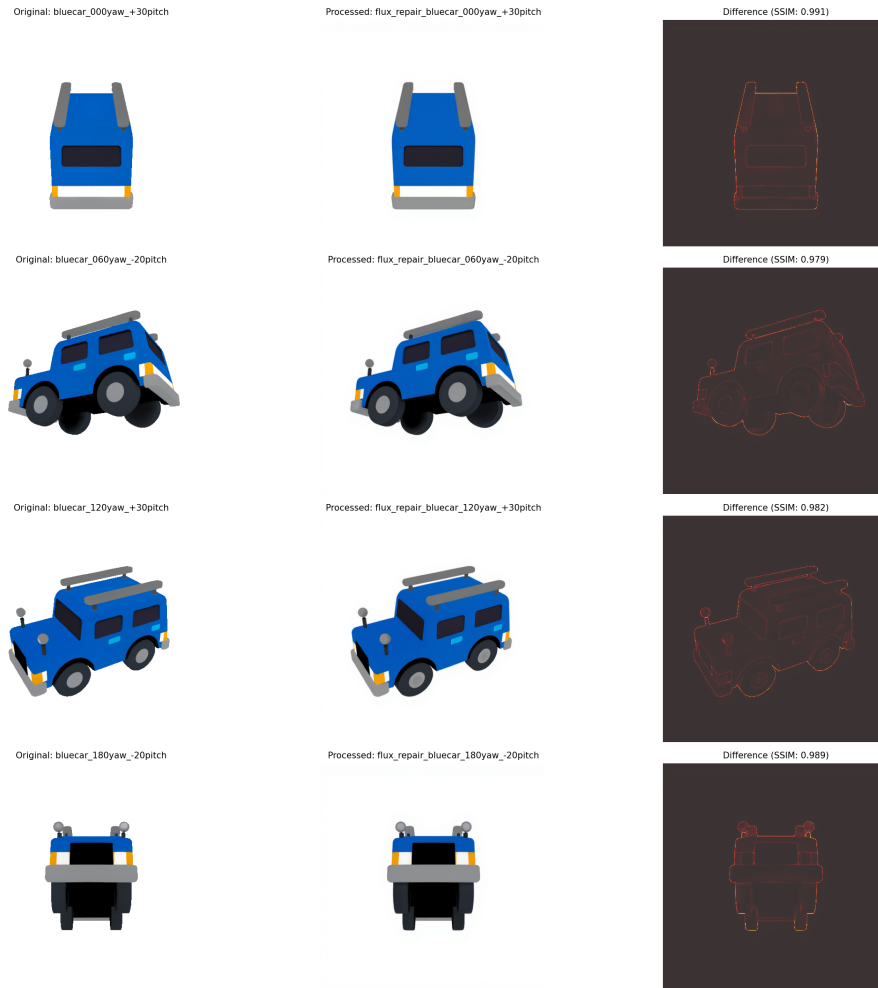


Fig. S3: Comparison between raw 3D renderings (left), refined results using fine-tuned FLUX-LoRA (middle), and their difference maps with SSIM scores (right) across multiple viewpoints. The high SSIM scores and localized difference maps indicate that the harmonization primarily removes appearance-level shading artifacts while preserving the underlying object structure.

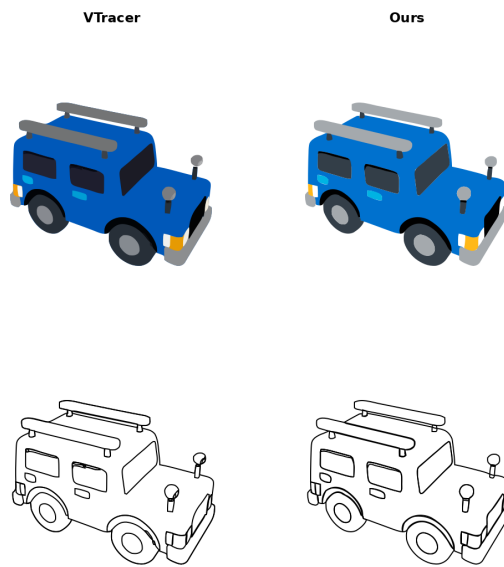


Fig. S4: Comparison between direct VTracer vectorization and our full vectorization pipeline. By combining part-aware segmentation, region-wise tracing, and palette alignment, our method suppresses noise-driven micro-paths and redundant intersections, yielding cleaner topology and more accurate color boundaries.

Table S1: Single-view comparison between direct VTracer and our full vectorization pipeline. The gains in SSIM, LPIPS, and ΔE_{2000} show that segmentation-guided tracing and palette alignment substantially improve SVG fidelity while preserving a compact vector structure.

Method	SSIM \uparrow	LPIPS \downarrow	ΔE_{2000} \downarrow	NumPaths \downarrow
VTracer (Direct)	0.833	0.0206	1.340	20.4
Ours	0.926	0.0200	0.408	19.75

D Full 360° Multi-View SVG Sequences

To comprehensively demonstrate the geometric stability and robust color consistency of SVG360, we present full 51-view turntable sequences for several representative objects in Figures S5 to S8. These uncurated grids show both the rendered SVGs and their underlying path topologies. Our method consistently avoids the structural flickering, shape collapse, and severe semantic drift that often plague purely 2D generative approaches or direct auto-tracing methods, maintaining high fidelity to the original SVG style across all viewing angles.

E Evaluation Metrics and Protocol

Our evaluation is divided into three parts:

- **SVG-centric statistics**, which measure the compactness and cross-view stability of the generated SVGs.
- **Multi-view continuity**, which evaluates whether adjacent views preserve smooth feature and perceptual transitions on the yaw-pitch grid.
- **Single-view raster-to-SVG fidelity**, which measures how faithfully each generated SVG reproduces its raster target.

These metrics are designed to jointly evaluate editability, structural consistency, color stability, and visual smoothness.

E.1 Common evaluation protocol

View set and notation. For each object, we evaluate a set of rendered viewpoints \mathcal{V} that matches the Adobe Turntable [1] configuration, with yaw sampled every 15° within its supported range and pitch levels in $\{-45^\circ, 0^\circ, +45^\circ\}$. For each view $v \in \mathcal{V}$, a method outputs an SVG S_v . We rasterize each SVG back into an image I_v using identical rendering settings across methods, including resolution, background, and antialiasing.

Adjacency on the yaw-pitch grid. We arrange all views into a 2D yaw-pitch grid. Let \mathcal{E}_{yaw} denote the set of yaw-adjacent pairs with the same pitch and consecutive yaw steps. Let $\mathcal{E}_{\text{pitch}}$ denote the set of pitch-adjacent pairs with the same yaw and consecutive pitch levels. We define the full adjacent-pair set as

$$\mathcal{E} = \mathcal{E}_{\text{yaw}} \cup \mathcal{E}_{\text{pitch}}.$$

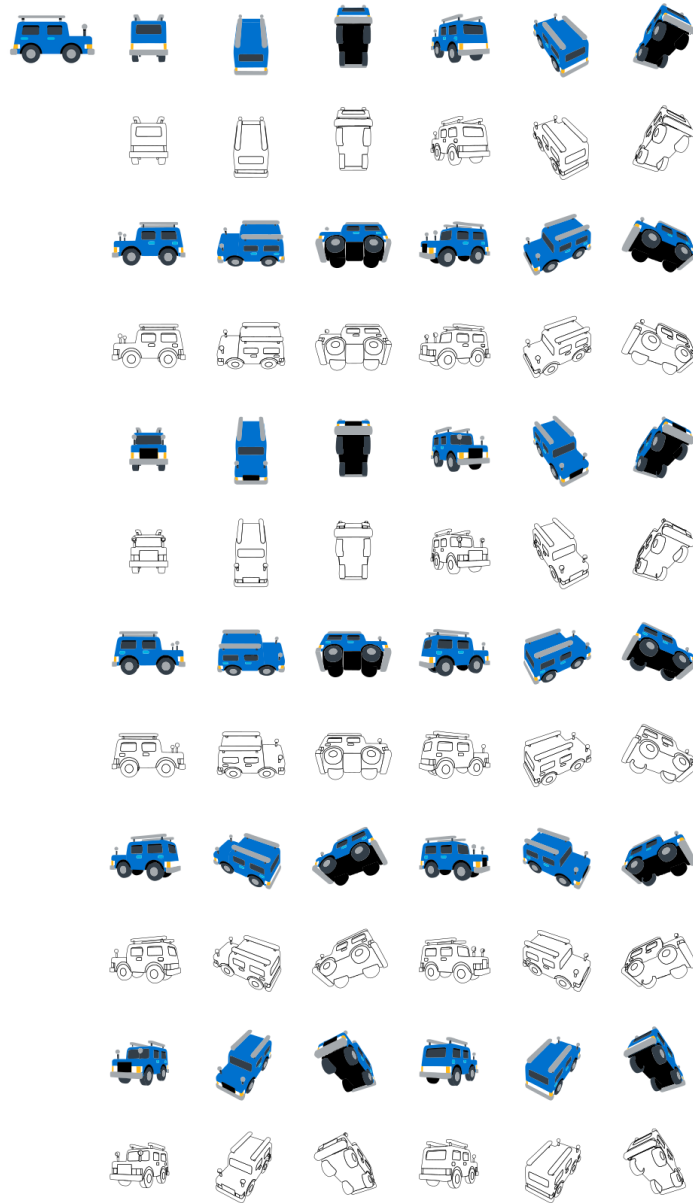


Fig. S5: Full multi-view sequence for “Blue Car”. Top rows show the rendered SVGs; bottom rows visualize the corresponding vector paths.

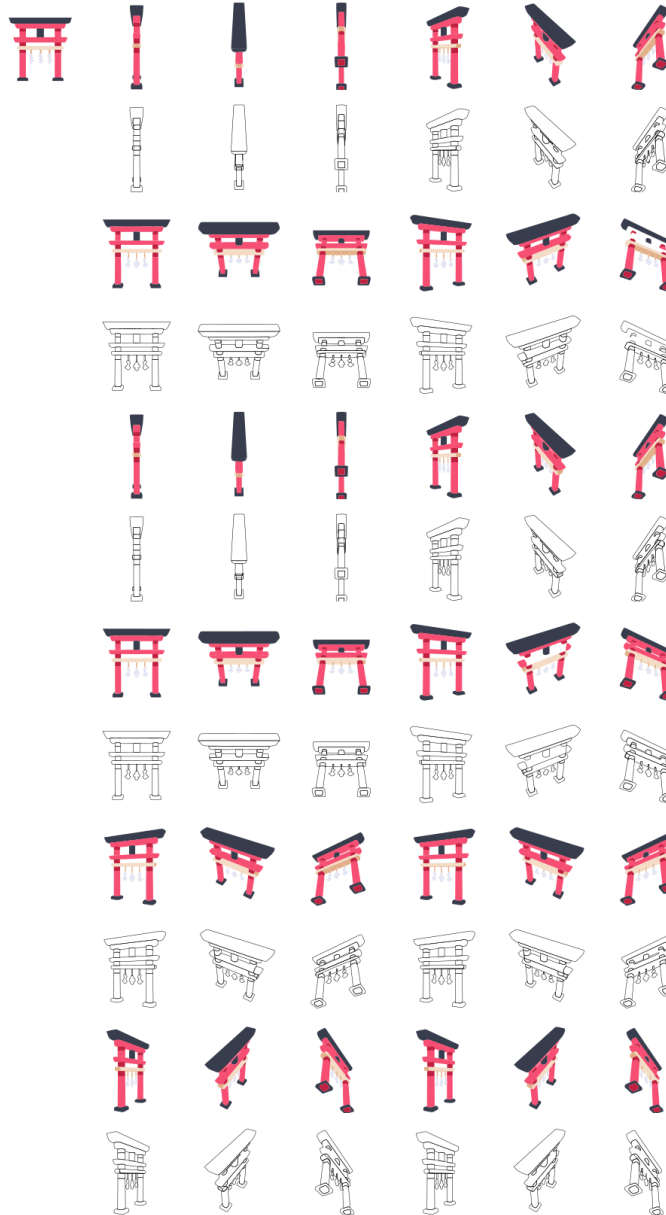


Fig. S6: Full multi-view sequence for “Torii Gate”. Top rows show the rendered SVGs; bottom rows visualize the corresponding vector paths.

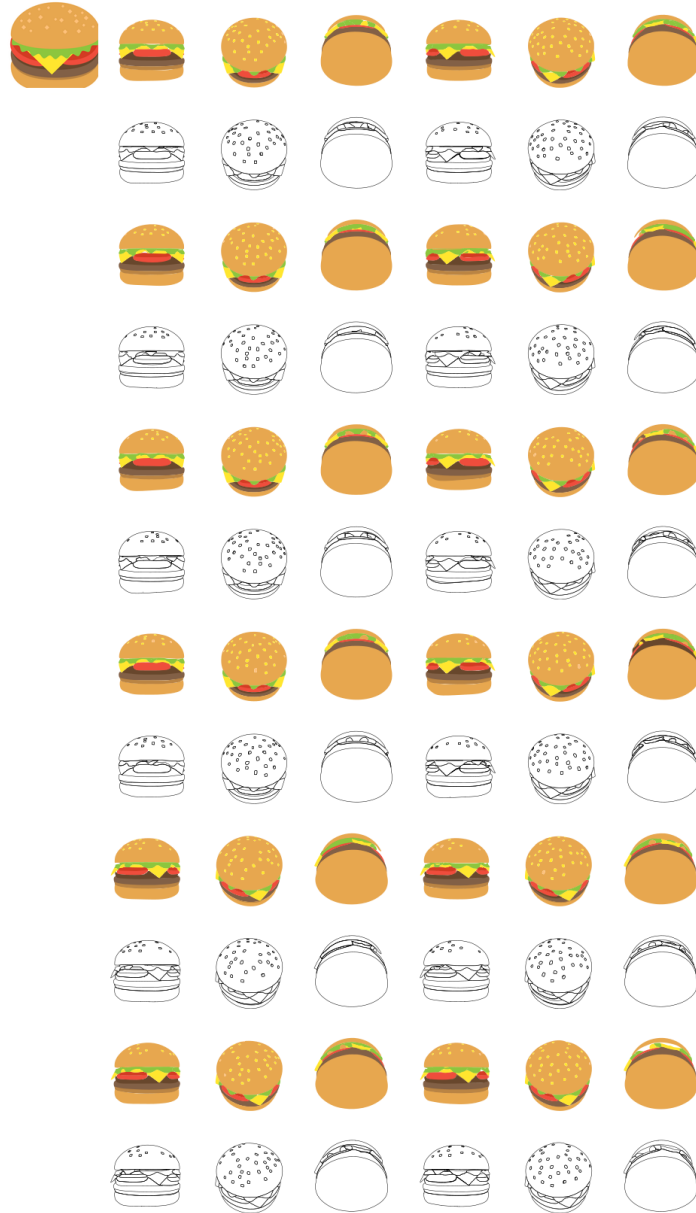


Fig. S7: Full multi-view sequence for “Hamburger”. Top rows show the rendered SVGs; bottom rows visualize the corresponding vector paths.

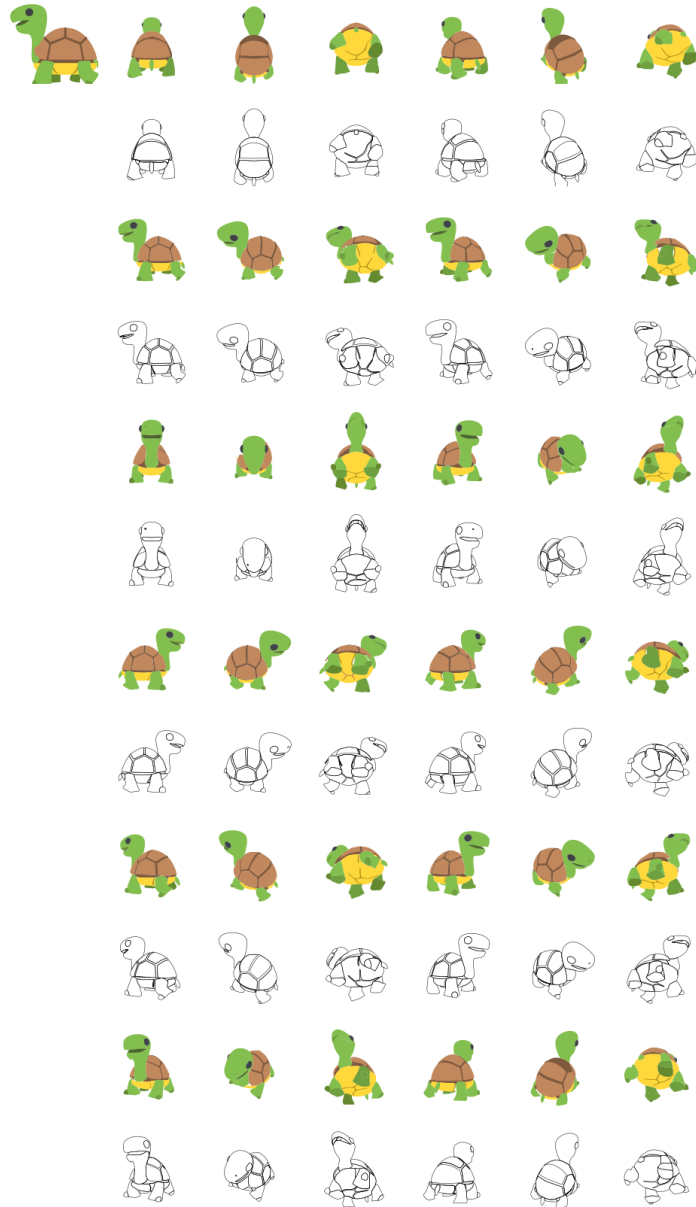


Fig. S8: Full multi-view sequence for “Turtle”. Top rows show the rendered SVGs; bottom rows visualize the corresponding vector paths.

Dataset aggregation. For metrics computed per object, we first compute the metric for each object and then report the average across all objects. For metrics computed per view or per adjacent pair, we first average within each object and then average across objects.

E.2 SVG-centric statistics

These metrics characterize the compactness and stability of generated multi-view SVG outputs.

Average number of paths \overline{N}_{path} . For each SVG S_v , we count the number of visible shape paths, excluding non-geometry elements such as `defs`, `clipPath`, and masks. Let $N_{path}(v)$ be the path count of view v . We define

$$\overline{N}_{path} = \frac{1}{|\mathcal{V}|} \sum_{v \in \mathcal{V}} N_{path}(v).$$

This metric reflects vector complexity and practical editability. Fewer paths usually indicate a more compact SVG, although this should be interpreted together with fidelity metrics.

Average number of colors \overline{N}_{color} . We extract all visible fill colors from the shape paths in S_v , represented in sRGB space. Let $N_{color}(v)$ be the number of unique fill colors in view v . We define

$$\overline{N}_{color} = \frac{1}{|\mathcal{V}|} \sum_{v \in \mathcal{V}} N_{color}(v).$$

This metric measures palette compactness. A smaller number of colors often suggests reduced spurious variation and better downstream editability.

Path-count stability $RMSE_{path}$. Let N_{path}^{in} be the number of visible shape paths in the input SVG. We compute the deviation of each generated view from the input complexity:

$$RMSE_{path} = \sqrt{\frac{1}{|\mathcal{V}|} \sum_{v \in \mathcal{V}} \left(N_{path}(v) - N_{path}^{in} \right)^2}.$$

This metric evaluates structural stability across views. A lower value indicates that the method preserves similar vector complexity under viewpoint changes.

Neighbor color-count change $\overline{\Delta N}_{color,nbr}$. For each adjacent pair $(v_i, v_j) \in \mathcal{E}$, we compute the absolute difference in the number of unique colors:

$$\overline{\Delta N}_{color,nbr} = \frac{1}{|\mathcal{E}|} \sum_{(v_i, v_j) \in \mathcal{E}} |N_{color}(v_i) - N_{color}(v_j)|.$$

This metric measures palette stability across neighboring views. Lower values indicate smoother color behavior under small viewpoint changes.

Perceptual color drift ΔE_{2000} on adjacent views. We use the CIEDE2000 distance [39] to measure perceptual color differences between corresponding regions in adjacent views. To ensure geometric alignment, corresponding regions are matched via an IoU-based heuristic. For a matched region pair (p, q) , let $\mu_{v,p}$ denote the mean Lab color of region p in view v . We define

$$\Delta E_{2000} = \frac{1}{|\mathcal{E}|} \sum_{(v_i, v_j) \in \mathcal{E}} \frac{1}{|\mathcal{M}_{v_i \rightarrow v_j}|} \sum_{(p, q) \in \mathcal{M}_{v_i \rightarrow v_j}} \Delta E_{00}(\mu_{v_i, p}, \mu_{v_j, q}).$$

Here, $\mathcal{M}_{v_i \rightarrow v_j}$ denotes the set of matched region pairs between adjacent views v_i and v_j . In practice, adjacent pairs with no valid region matches are excluded from the computation. This metric captures perceptual color consistency across neighboring views. Lower values indicate less viewpoint-dependent color drift.

E.3 Multi-view continuity

We evaluate whether neighboring views change smoothly on the yaw-pitch grid. Following the main paper, we report Yaw and Pitch scores by averaging over the corresponding adjacency sets, and Overall scores by averaging over all adjacent pairs on the full grid.

DINO feature consistency. For an adjacent image pair (I_{v_i}, I_{v_j}) , we extract DINOv2 [31] patch-token features $\{f_{v_i}^p\}_{p=1}^P$ and $\{f_{v_j}^q\}_{q=1}^P$. For each patch p in I_{v_i} , we find its nearest patch in I_{v_j} using cosine similarity:

$$q^*(p) = \arg \max_q \frac{\langle f_{v_i}^p, f_{v_j}^q \rangle}{\|f_{v_i}^p\| \|f_{v_j}^q\|}.$$

The adjacent-pair DINO score is defined as

$$S_{\text{DINO}}(I_{v_i}, I_{v_j}) = \frac{1}{P} \sum_{p=1}^P \frac{\langle f_{v_i}^p, f_{v_j}^{q^*(p)} \rangle}{\|f_{v_i}^p\| \|f_{v_j}^{q^*(p)}\|}.$$

We then compute

$$\begin{aligned} \text{DINO}_{\text{Yaw}} &= \frac{1}{|\mathcal{E}_{\text{yaw}}|} \sum_{(v_i, v_j) \in \mathcal{E}_{\text{yaw}}} S_{\text{DINO}}(I_{v_i}, I_{v_j}), \\ \text{DINO}_{\text{Pitch}} &= \frac{1}{|\mathcal{E}_{\text{pitch}}|} \sum_{(v_i, v_j) \in \mathcal{E}_{\text{pitch}}} S_{\text{DINO}}(I_{v_i}, I_{v_j}), \end{aligned}$$

and

$$\text{DINO}_{\text{Overall}} = \frac{1}{|\mathcal{E}|} \sum_{(v_i, v_j) \in \mathcal{E}} S_{\text{DINO}}(I_{v_i}, I_{v_j}).$$

This metric captures feature-level structural continuity across adjacent views. Higher values indicate smoother transitions.

DreamSim perceptual similarity. Using the same adjacency sets, we replace the pairwise similarity function with DreamSim [9]:

$$\text{DreamSim}_{\text{Yaw}} = \frac{1}{|\mathcal{E}_{\text{yaw}}|} \sum_{(v_i, v_j) \in \mathcal{E}_{\text{yaw}}} \text{DreamSim}(I_{v_i}, I_{v_j}),$$

$$\text{DreamSim}_{\text{Pitch}} = \frac{1}{|\mathcal{E}_{\text{pitch}}|} \sum_{(v_i, v_j) \in \mathcal{E}_{\text{pitch}}} \text{DreamSim}(I_{v_i}, I_{v_j}),$$

and

$$\text{DreamSim}_{\text{Overall}} = \frac{1}{|\mathcal{E}|} \sum_{(v_i, v_j) \in \mathcal{E}} \text{DreamSim}(I_{v_i}, I_{v_j}).$$

This metric captures perceptual continuity in a way that better aligns with human visual judgment. Higher values indicate smoother adjacent-view appearance.

E.4 Single-view raster-to-SVG fidelity

These metrics evaluate reconstruction quality in the single-view setting, independently of cross-view propagation.

Rendering for evaluation. For each predicted SVG S , we rasterize it into an image I_{svg} at the same resolution as the target raster image I_{in} , using identical background and antialiasing settings. All metrics below are computed between I_{svg} and I_{in} , and the final reported score is the average over the evaluation set.

SSIM. We compute the structural similarity index (SSIM) [50]:

$$\text{SSIM}(I_{\text{svg}}, I_{\text{in}}).$$

This metric measures structural fidelity and local contrast preservation. Higher values indicate better reconstruction quality.

LPIPS. We compute LPIPS [60] using the standard pretrained perceptual network:

$$\text{LPIPS}(I_{\text{svg}}, I_{\text{in}}).$$

This metric captures perceptual reconstruction quality beyond raw pixel matching. Lower values indicate better perceptual fidelity.

Single-view ΔE_{2000} . We compute the mean CIEDE2000 distance [39] in Lab space between I_{svg} and I_{in} , optionally restricted to a foreground region:

$$\Delta E_{2000}^{\text{sv}} = \frac{1}{|\Omega|} \sum_{x \in \Omega} \Delta E_{00}(\text{Lab}(I_{\text{svg}}(x)), \text{Lab}(I_{\text{in}}(x))),$$

where Ω denotes the evaluation region, either the full image or a foreground mask. This metric measures perceptually meaningful color fidelity. Lower values indicate better color reproduction.

Path count (single view). For each single-view SVG output, we report the number of visible shape paths. This complements raster fidelity metrics by indicating vector complexity and editability.

F Additional Remarks

The above metrics are designed to evaluate complementary aspects of multi-view SVG generation. SVG-centric statistics focus on compactness and stability of the vector representation. Multi-view continuity metrics evaluate smoothness across adjacent views on the yaw-pitch grid. Single-view SSIM, LPIPS, and $\Delta E_{2000}^{\text{sv}}$ measure the fidelity of the vectorized view itself. Together, these metrics provide a more complete assessment than either raster fidelity or vector compactness alone.